Arctic Science

OPEN ACCESS | Article

Shoreline change rates and land to sea sediment and soil organic carbon transfer in eastern Parry Peninsula from 1965 to 2020 (Amundsen Gulf, Canada)

Rodrigue Tanguy[a], **Dustin Whalen**[b], **Gonçalo Prates**[a,c], **and Gonçalo Vieira**[a]

[a]Centre of Geographical Studies, TERRA Associated Laboratory, Institute of Geography and Spatial Planning, University of Lisbon, Lisbon, Portugal; [b]Natural Resources Canada, Dartmouth, Canada; [c]Superior Institute of Engineering, University of Algarve, Faro, Portugal

Corresponding author: **Rodrigue Tanguy** (email: rodrigue.tanguy@edu.ulisboa.pt)

Abstract

As the Arctic is warming, permafrost coasts are eroding faster, threatening coastal communities, habitats, and altering sediment and nutrient budgets. The western Canadian Arctic is eroding at a rapid pace; however, little is known on changes occurring in the Amundsen Gulf area. This study was conducted in the eastern coast of Parry Peninsula, a neglected rock-dominated coastal area. We used orthorectified aerial photos of 1965 and 1993 and very high-resolution satellite imagery of 2020 to manually delineate the shoreline according to backshore and foreshore centered approaches. Shoreline change rates were calculated and sediment and organic carbon transfer from land to sea estimated using digital elevation model, the Northern Circumpolar Soil Carbon Database, and ground ice content. The results show a mean erosion rate of 0.12 m/yr for the backshore zone and 0.16 m/yr for the foreshore zone, with increasing erosion in the Paulatuk Peninsula in recent decades. The average sediment transfer from land to sea was 20 m^3/m/yr and the soil organic carbon (SOC) flux was 7 kg C/m/yr. We highlight the importance of using the cliff-top as shoreline reference to accurately estimate sediment and SOC transfers, an approach neglected in automatic shoreline delineation techniques based on remote sensing imagery using the waterline.

Key words: coastal dynamics, permafrost, Darnley Bay, carbon fluxes, remote sensing

Résumé

À mesure que l'Arctique se réchauffe, les côtes de pergélisol s'érodent plus rapidement, menaçant les communautés locales et les habitats côtiers. L'Arctique canadien occidental s'érode à un rythme rapide ; cependant, on sait peu de choses sur les changements qui se produisent dans la région du golfe d'Amundsen. Cette étude a été menée sur la côte Est de la péninsule de Parry. Nous avons utilisé des photos aériennes de 1965 et 1993 et des images satellites de très haute résolution de 2020 pour délimiter manuellement le trait de côte selon des approches basées sur l'arrière-côte et l'estran. L'évolution du trait de côte a été calculée entre 1965 et 2020 et le transfert de sédiments et de carbone organique vers les eaux côtières a été estimé à l'aide d'un modèle numérique de terrain et des bases de données sur la teneur en carbone organique et en glace du pergelisol. Les résultats révèlent un taux d'érosion moyen de 0,12 m/an pour la zone d'arrière-côte et de 0,16 m/an pour la zone d'estran, avec des taux d'érosion qui ont doublés le long de la péninsule de Paulatuk au cours des dernières décennies. Le transfert moyen de sédiments de la terre vers la mer était de 20 m^3/m/yr et le flux de carbone organique du sol était de 7 kg C/m/an. Nous soulignons l'importance d'utiliser le haut de la falaise comme référence du trait de côte pour estimer avec précision les transferts de sédiments et de carbone organique, une approche négligée dans les methodes de délimitation automatiques du trait de côte basées sur des images de télédétection qui se réfèrent au bas d'estran ou à la limite entre terre et mer.

Mots-clés : baie de Darnley, carbone organique, dynamique côtière, pergélisol, télédétection

1. Introduction

The unprecedented warming of the Arctic in the last decades is strongly altering permafrost landscapes due to ground ice thawing. Permafrost coasts are particularly vulnerable to temperature variations and their retreat rates are increasing in several regions (IPCC 2019; Berry et al. 2021). The average coastal erosion rate in the Arctic is 0.5 m/yr (Lantuit et al. 2012), but these rates are heterogeneous and dependent on various factors. The sea ice decline increases the impact of storms and waves on Arctic coasts; moreover,

sea-level rise and the loss of bluff cohesion by thawing permafrost coasts are not only exacerbating erosion, threatening infrastructures and local communities but also playing a major role in the release of soil organic carbon (SOC) to the atmosphere and coastal waters (Irrgang et al. 2018). Within the Canadian Arctic, most studies have been concentrated in the Beaufort Sea along the Yukon coast (especially Qikiqtaruk/Herschel Island), the Mackenzie delta, and the Tuktoyaktuk Peninsula (Harper 1990; Manson et al. 2005; Solomon 2005; Jones et al. 2009; Lantuit et al. 2012; Obu et al. 2017; Irrgang et al. 2018), but systematic research is lacking eastward.

The analysis of aerial and satellite imagery allows to assess rapid coastal retreat and its spatial and intra-annual variability. Several studies have shown that most of the Beaufort Sea coast is subject to erosion and is retreating faster in recent years (Jones et al. 2009; Lantuit et al. 2012; Cunliffe et al. 2019; Whalen et al. 2022). Rapid and extensive erosion is occurring not only in Qikiqtaruk/Herschel Island, which presents an average erosion rate of 2.2 m/yr (Cunliffe et al. 2019), but also in the Mackenzie Estuary, with annual retreat rates between 2.1 and 6.1 m/yr, with 22.5 m/yr reported in some sectors (Solomon 2005; Obu et al. 2017) and over 40 m/yr at Pelly Island (Malenfant et al. 2022). The high retreat rates are mainly associated with retrogressive thaw slumps, and sectors with widespread bluff block failure governed by ground ice thawing. The Yukon coast and Tuktoyaktuk Peninsula present lower retreat rates, averaging 0.7 m/yr (O'Rourke 2017; Irrgang et al. 2018; Whalen et al. 2022). The highest erosion rates are associated with ice-rich permafrost and unconsolidated sediments, while permafrost in consolidated bedrock remains stable (Lantuit et al. 2012).

The factors explaining the spatial variability of erosion rates depend mainly on geology, ground ice content, cliff height, and orientation. The temporal variability of erosion is explained by ice-free season length variation, storminess and wave height, relative sea-level rise, and precipitations (Hequette and Barnes 1990; Galley et al. 2008; Obu et al. 2017; Lim et al. 2020; Berry et al. 2021). Moreover, the large amount of organic carbon and mercury stored in permafrost soils can be released into coastal waters and the atmosphere (Schuster et al. 2018; Tanski et al. 2019), influencing the biogeochemical cycle of carbon, and potentially impacting aquatic resources and human health. Volumetric erosion analysis using digital elevation models (DEMs) and planimetric retreat rates are efficient methods for the estimation of sediment release and SOC fluxes into the nearshore zone (Obu et al. 2016).

Sankar et al. (2019) provided a first assessment of the coastal dynamics and associated driving factors in the Paulatuk Peninsula, an Inuvialuit settlement located in the south of Darnley Bay. This investigation showed that erosion increased along the western and eastern coastlines of the peninsula from 2000 to 2016. The authors suggest that increasing storminess and wind speed coupled with increasing sea surface and air temperatures affected the sea ice regime and permafrost conditions, leading to the increasing erosion rates.

This study focuses on the mouth of the Amundsen Gulf, on the eastern coast of Parry Peninsula, which is included in the Anguniaqvia Niqiqyuam Marine Protected Area (ANMPA), as well as the Inuvialuit settlement of Paulatuk and numerous traditional fishing and hunting areas (Fast et al. 2001). We applied remote sensing methods using very high-resolution satellite imagery and historic aerial photos to (1) quantify coastal changes at the regional scale as a function of the type of coast, comparing the use of the backshore and foreshore as a basis for defining the shoreline; (2) investigate the spatiotemporal variation of coastal changes from 1965 to 2020, and (3) estimate sediment volume and SOC transfer from land to sea associated with cliff-top retreat.

2. Study area

Parry Peninsula is approximately 150 km long and 60 km wide and is limited in the west by Franklin Bay and in the east by Darnley Bay (Fig. 1). The Inuvialuit settlement of Paulatuk is located in Darnley Bay to the southeast of the peninsula. Cape Parry in the north is home to the Distant Early Warning Line site, while the limestone cliffs are important bird nesting areas. Cape Parry is classed as a migratory bird sanctuary since 1961 (Latour 2008). The westward area of Darnley Bay is part of the Marine Protected Area since 2009 due to its important ecological and biological values (Paulic et al. 2011). It is the habitat of various mammals, such as the beluga and the bowhead whale, but also for Arctic Char. The region is in the continuous permafrost zone and the bedrock is Mesozoic to Paleozoic carbonates, shales, and sandstones (Kerr 1994). Parry Peninsula is lying below 30 m and is made of dolostone (Figs. 1 and 2B), covered by continuous fluvioglacial deposits composed of silty sand and clay diamictons. The prominent headlands of Cape Parry and Bennett Point are characterized by 20 m high limestone cliffs (Environment Canada 2015). The area from Cape Parry to Clapperton Island shows a thermokarst topography landscape on which recent marine transgression flooded basins forming numerous bays (Paulic et al. 2011). The sector from Clapperton Island to Paulatuk is constituted of Cenozoic morainal deposits forming a more linear coast (Figs. 1 and 2A). Paulatuk and the Hornaday and Broke River deltas are fluvial and lacustrine terraces (Kerr 1994).

The prevailing winds are influenced by the Amundsen Gulf and blow from the east, while katabatic winds are southerly (Mackay and Burn 2005). Cape Parry is exposed to northwest storm swells and therefore shelters the interior of Darnley Bay. Coastal dynamics in Darnley Bay is limited to the brief ice-free season, lasting from July to October (Fequet et al. 2011). Currents and waves are wind driven and are only generated in the open-water season. Coupled with alongshore drift, they are able to remobilize shelf sediments and build depositional coastal forms (Atkinson et al. 2016). The region is characterized by a microtidal range that extends from 0.3 to 0.5 m (Fequet et al. 2011).

The landcover is dominated by low tundra dominated sparse vegetation, reflecting the extreme climatic conditions. The mean annual temperature at Cape Parry is about −11.4 and −9.3 °C at Paulatuk (Environment Canada 2014). The hottest month (July) presents a mean

Fig. 1. Regional setting of Parry Peninsula and its geology (modified from Yorath et al. 1975). The contour equidistance is 5 m. Map projection: WGS 84/UTM zone 10.

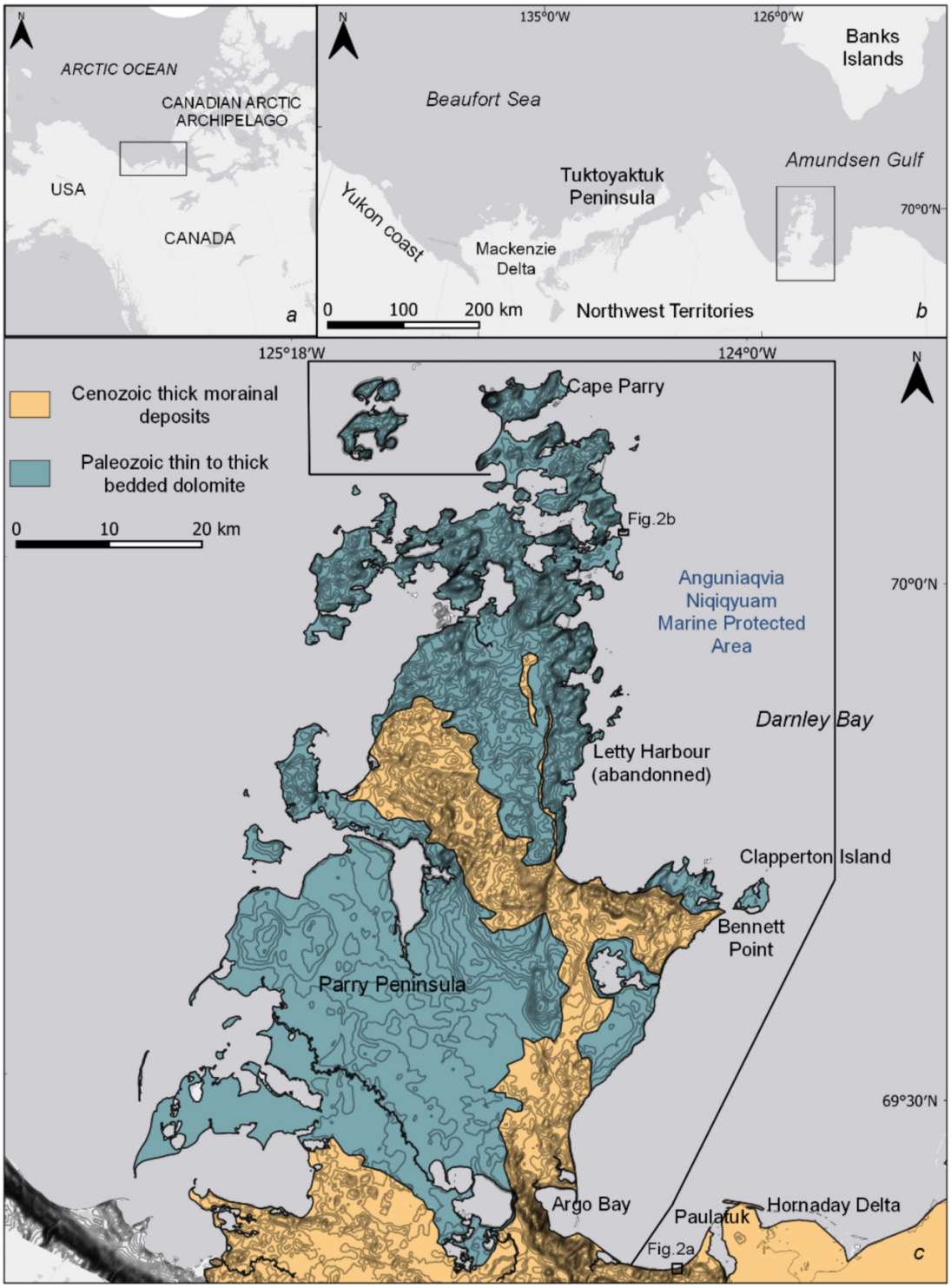

air temperature of +6.7 °C, while the coldest month (February) is −27.5 °C. Extreme temperatures vary from −47.2 °C (January) to +23.9 °C (July). Most precipitation is concentrated between July and October and associated with maritime air masses. The mean annual amount of precipitation is 213 mm in Paulatuk and 161 mm in Cape Parry with average maximum of 34.5 mm in August (Environment Canada 2014).

3. Methods

3.1. General approach

This work combines photogrammetric and remote sensing techniques to assess coastal changes in the eastern coast of Parry Peninsula from 1965 to 2020 (Fig. 3). The analysis was based on the processing of aerial photography surveys

Fig. 2. Oblique pictures from the study area. (A) Unconsolidated moraine deposits located in the southern portion of Darnley Bay. (B) Dolomite beds in the North of Parry Peninsula. Photos: © W. Murray and © Government of Northwest Territories.

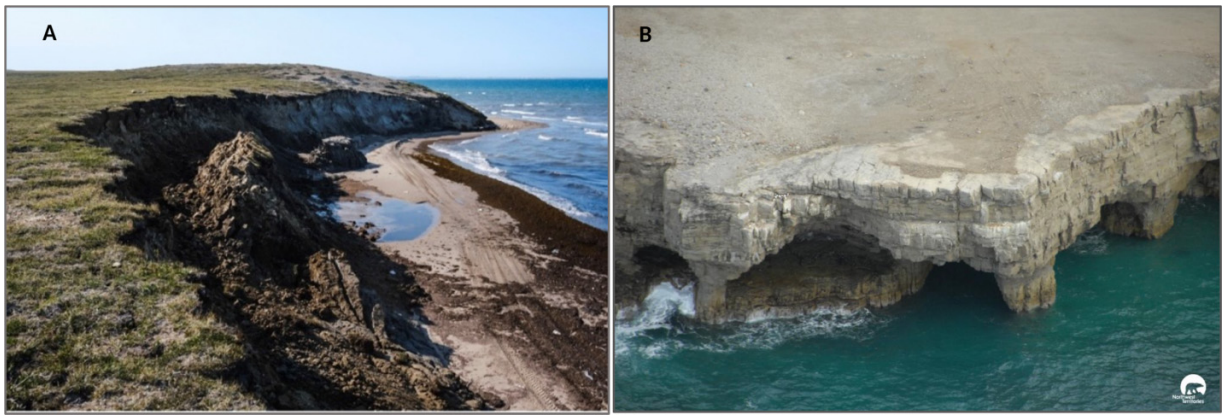

Fig. 3. Analytical workflow for assessing the coastline dynamics of Darnley Bay.

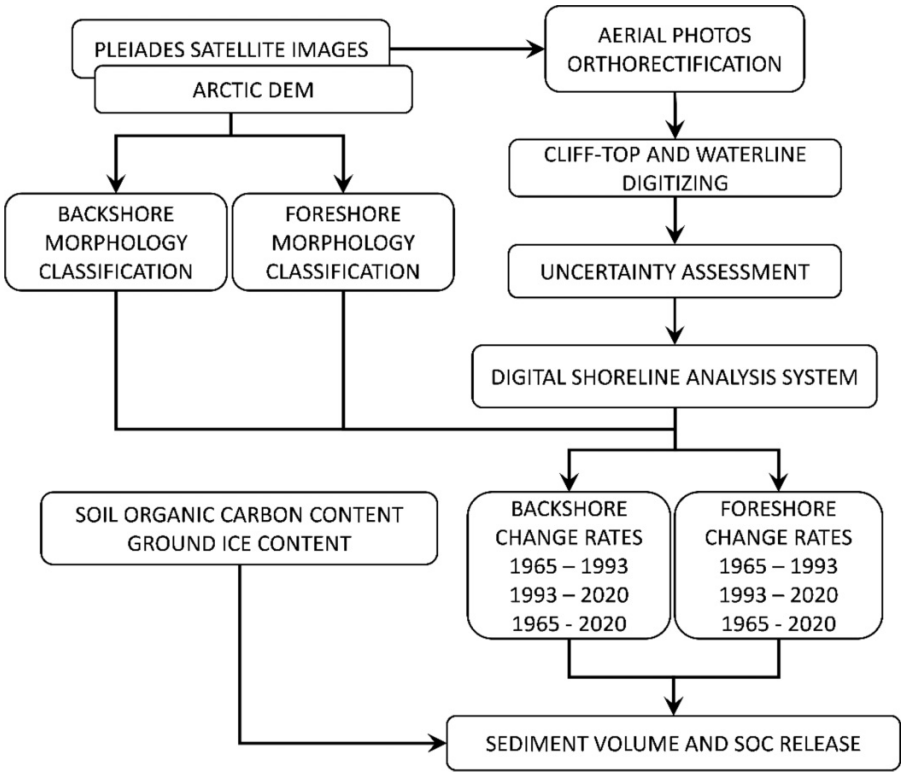

of 1965 and 1993 (Energy, Mines and Resources of Canada, distributed by Natural Resources Canada) and very high-resolution (0.5 m) Pléiades satellite imagery from 2020 (CNES and Airbus) (Table 1). This allowed for the spatiotemporal characterization of shoreline changes. The 2 m resolution Arctic Digital Elevation Model (ArcticDEM) was used for pre-processing the aerial imagery and for the extraction of morphometric data. The coast was classified by interpretation of the 2020 Pléiades imagery and using the modified classification scheme adopted by the Geological Survey of Canada and Environment Canada (Sergy 2008; Environment Canada 2015). The shoreline change rates, the coastal classification, and the morphometric data were used together with the 1 km resolution grids of ground ice content (O'Neill et al. 2019) and soil organic carbon content (SOCC) (Hugelius et al. 2013) for the estimation of sediment volume and SOC transfer from land to sea. Differences in the calculation of the latter two using the backshore- and the foreshore-derived shorelines as proxies are discussed, as well as their implications for remote sensing analysis.

3.2. Image processing and shoreline digitizing

A total of 27 monochrome aerial photos from 1965 and 1993 have been georeferenced and orthorectified with the construction of rational polynomial coefficients (RPCs) using the 2 m DEM (ArcticDEM) in ENVI 5.6.

Table 1. Characteristics and errors related to processed images.

Data	Acquisition date	Number of scenes	Scale	Bands	Pixel size (m)	Mean RMSE (m)	Coastline position uncertainty (m)
Aerial photography (black and white)	Aug. 1965	18	1:50 000	1	0.6	2.51	2.58
	Aug. 1993	9	1:5000	1	0.6	1.12	1.27
Pléiades (multispectral, pansharpened)	Aug. 2020	9	–	4	0.5	0.35	0.61

Note: The Pléiades RSME is issued by the image quality commitments (Airbus).

Orthorectification processing was applied to remove internal and external distortions, relief effects and to assign correct geographical coordinates to the images. To do this, the internal orientation was constructed from the camera specifications: model, focal length, and fiducial mark coordinates. The construction of the external orientation was done by selecting common reference points (GCPs) between the master Pléiades images and the aerial photos, with the elevation obtained from the ArcticDEM. This procedure allowed calculating the RPCs for each image. The last step was the refinement of the RPC model in ENVI by selecting GCPs and estimating the root-mean-square error (RMSE in meters) for the X, Y, and Z to calculate the horizontal and vertical accuracy relative to the Pléiades imagery. The final products were orthophotos in TIFF format with 0.6 m resolution. The shorelines were then digitized using as consistent references both the cliff-top line/vegetation line and the waterline. The objective was assessing coastal changes occurring within the backshore zone, defined as the zone backing the cliff-top line, and within the foreshore zone, corresponding to the zone between the waterline and the cliff foot or vegetation line (Fig. 4). The 1993 aerial photos were only available of the sector from the south of Argo Bay to Paulatuk Peninsula and hence only there we could compare two periods.

Tidal effect could induce an error in the delineation of the shoreline, especially along low-lying terrain, such as tundra flats. We were not able to find the exact water height of the tidal phase now of image acquisition. The Pléiades scenes were acquired between June and August 2020 with tides ranging from 0.3 to 0.5 m during this period. Due to their microtidal character, we did not include the tide effect in our calculations. Moreover, aerial and satellite imagery has been visually inspected for the detection of energetic marine conditions that could influence the position of the waterline. However, due to the protected character of this coastline to the prevailing swells, swell crest and swash have been detected on only 5 km of north exposed coast at Clapperton Island and Bennett Point sector with the 2020 imagery.

3.3. Shoreline change rate uncertainty assessment

The imagery used for the shoreline extraction shows intrinsic errors, which need to be quantified to assess the significance of shoreline changes. In this study, the shoreline position uncertainty (U_{SP}) was calculated for each shoreline as shown in eq. 1 (see Obu et al. 2016; Irrgang et al. 2018; Cunliffe et al. 2019)

$$U_{SP} = \sqrt{E_R^2 + E_G^2} \quad (1)$$

where U_{SP} is shoreline position uncertainty (m), E_R is the resolution error of the satellite imagery (pixel size, m), and U_G is the horizontal accuracy error (RMSE, m). The shoreline change rate uncertainty (U_{CR}) was computed using the shoreline position uncertainty for each shoreline and the period between both shoreline dates in eq. 2. The tidal effect has not been included in the calculations accounting for the minor changes associated with the microtidal range occurring in the region (0.3–0.5 m).

$$U_{CR} = \frac{\sqrt{U_{SP1}^2 + U_{SP2}^2}}{T_2 - T_1} \quad (2)$$

3.4. Coastal classification

The coastal landforms were classified in a two-tier system dividing the backshore and the foreshore zones and describing their geomorphological and sedimentary characteristics (Table 2; Fig. 5). The backshore includes (a) rocky cliffs, (b) rocky slope, (c) tundra cliffs, and (d) tundra slopes, and the foreshore includes (e) active rocky cliffs, (f) rocky platforms, (g) mixed sediment beaches and spits, (h) pebble and cobble beaches, (i) sandy beaches, (j) inundated low-lying tundra, and (k) peat shorelines. The spatial classification of the coastal landforms was made through interpretation of the Pléiades satellite imagery of 2020 and of the ArcticDEM, in combination with the classification of Sergy (2008) done by videography analysis and published in the Regional Sensitivity Atlas by Environment Canada (2015). The latter allowed to classify accumulation landforms according to grain size, which was not possible to determine from the interpretation of the Pléiades imagery alone.

3.5. Shoreline change rates

The cliff-top/vegetation line and the waterline were manually digitized for each year to perform the shoreline change analysis using ArcGIS 10.4 with the Digital Shoreline Analysis System (DSAS) v5.0 extension in ArcMap (Himmelstoss et al. 2018). Transects perpendicular to the coast at 40 m intervals were used to calculate shoreline evolution rates from 1965 to 2020. Between Argo Bay and Paulatuk Peninsula an extra time step was added for 1993 (Table 3). The calculation of the

Fig. 4. Zonal definition of the backshore and foreshore zones based on detectable shoreline references. Left: oblique ground image in the southwest of Paulatuk. Right: PLEIADES © CNES, 2020, distribution Airbus DS.

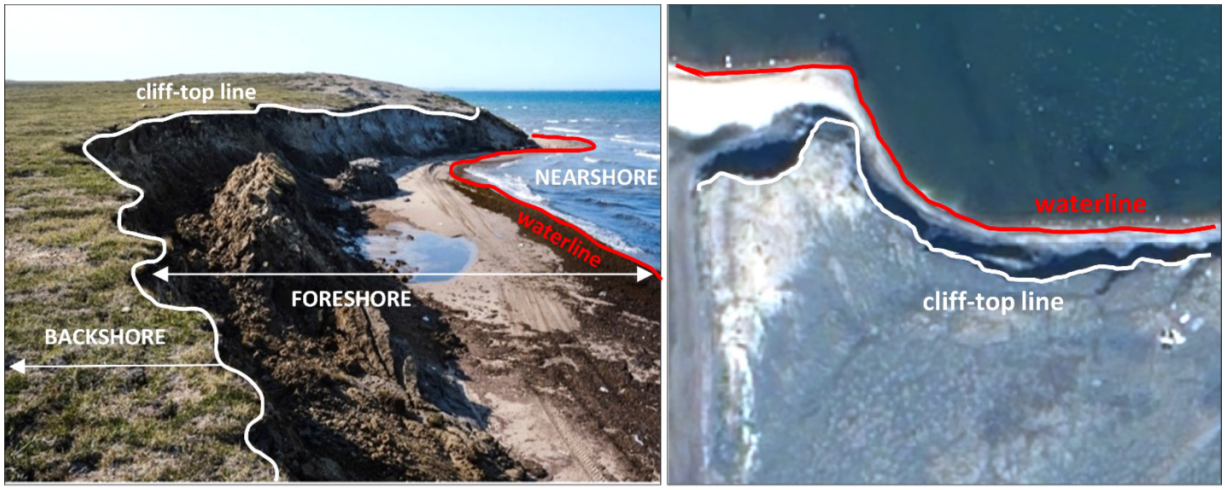

Table 2. Coastal landforms classification along the eastern coast of Parry Peninsula.

		Definition
Backshore	Rocky cliff (a)	Vertical outcrops of consolidated rock under the influence of marine action or protected by beaches. Erosion can create slots, caves, arches, and slopes.
	Rocky slope (b)	Outcrops of consolidated rock showing gradual slope face toward the sea. They can be fronted by a beach or a rocky platform.
	Tundra cliff (c,i)	Unconsolidated vertical cliffs composed of silty clays and organic material and characterized by high ground ice content and can be adjacent to ice-wedge polygon networks or slumps. These coastlines are sensitive to thermal abrasion and wave action.
	Tundra slope (d)	Tundra slope face generally lined by narrow beaches of gravel or sand. The principal processes of mass loss for ice-poor tundra cliffs are surficial washout and landslides observable by interfluvial crests.
Foreshore	Active rocky cliff (a)	Vertical outcrops of consolidated rock under the influence of marine action where erosion can create slots, caves, arches, and slopes.
	Rocky platform (e)	Flat to slightly seaward sloping surface where material is released by cryoclastic processes, sea ice scouring, and carved by the waves, in a rock with a minimum of resistance and ending at the top of the foreshore on a more or less pronounced coastal cliff escarpment.
	Mixed sediment beach and spit (f)	Sedimentary accumulation forms, mainly present along the coast. They are composed of mixed sediments ranging from pebbles to sand. These forms are subject to seasonal remobilization by the action of sea ice, waves, and alongshore currents.
	Pebble/cobble beach (g)	Beach made of fragmented material ranging from 4 to 64 mm (pebble) and 64 to 256 mm (cobble) is dominant originating from adjacent head cliffs due to weathering and solifluction.
	Sandy beach (h)	Mobile sediment stretches where marine actions have sorted grain size ranging from 0.0665 to 2.0 mm of diameter. These features are often anchored at the end of stable headlands forming spits or barrier beaches.
	Inundated low-lying tundra (i)	Very low-lying coastal tundra that is inundated or submerged by marine waters during high spring tides or wind-driven surges. These areas are not located in the intertidal zone. They are marked by a pattern of regular geometric patterns of the ice-wedge polygons and shallow water ponds.
	Peat shoreline (j)	Low-lying coastline made of peat substrate made of soil and organic matter. These coasts are sensitive to thawing process and erosion.

Note: The foreshore classification is based on the Northern Canada Coastline Classification (Sergy 2008). Examples of the landforms are shown in Fig. 5.

end point rate (EPR) gives the annual rate of change in meters per year for the backshore and the foreshore zones. When only two coastlines are available, the EPR is still a good index for assessing kinematics. Erosion is expressed by negative values and accretion by positive values (Himmelstoss et al. 2018).

3.6. Sediment volume and SOC transfers from land to sea

Aiming at assessing the mass transfers from land to sea following coastal erosion, we calculated the annual sediment volume and SOC release per meter of coast using cliff-top

Fig. 5. Coastal landforms of eastern Parry Peninsula, typical of the backshore and foreshore classification (Table 2; Fig. 6), representing (*a*) rocky cliff and arches, (*b*) rocky slope and barrier beach, (*c*) sandy tundra cliff fronted by beach, (*d*) tundra slope with interfluvial crests and fronting beach, (*e*) rocky platform and beach, (*f*) mixed sediment spit with ridges, (*g*) pebble beach fronting tundra slope, (*h*) sandy beach fronting tundra cliff, (*i*) inundated low-lying tundra, and (*j*) peat shore. Source: © Government of Northwest Territories, 2009.

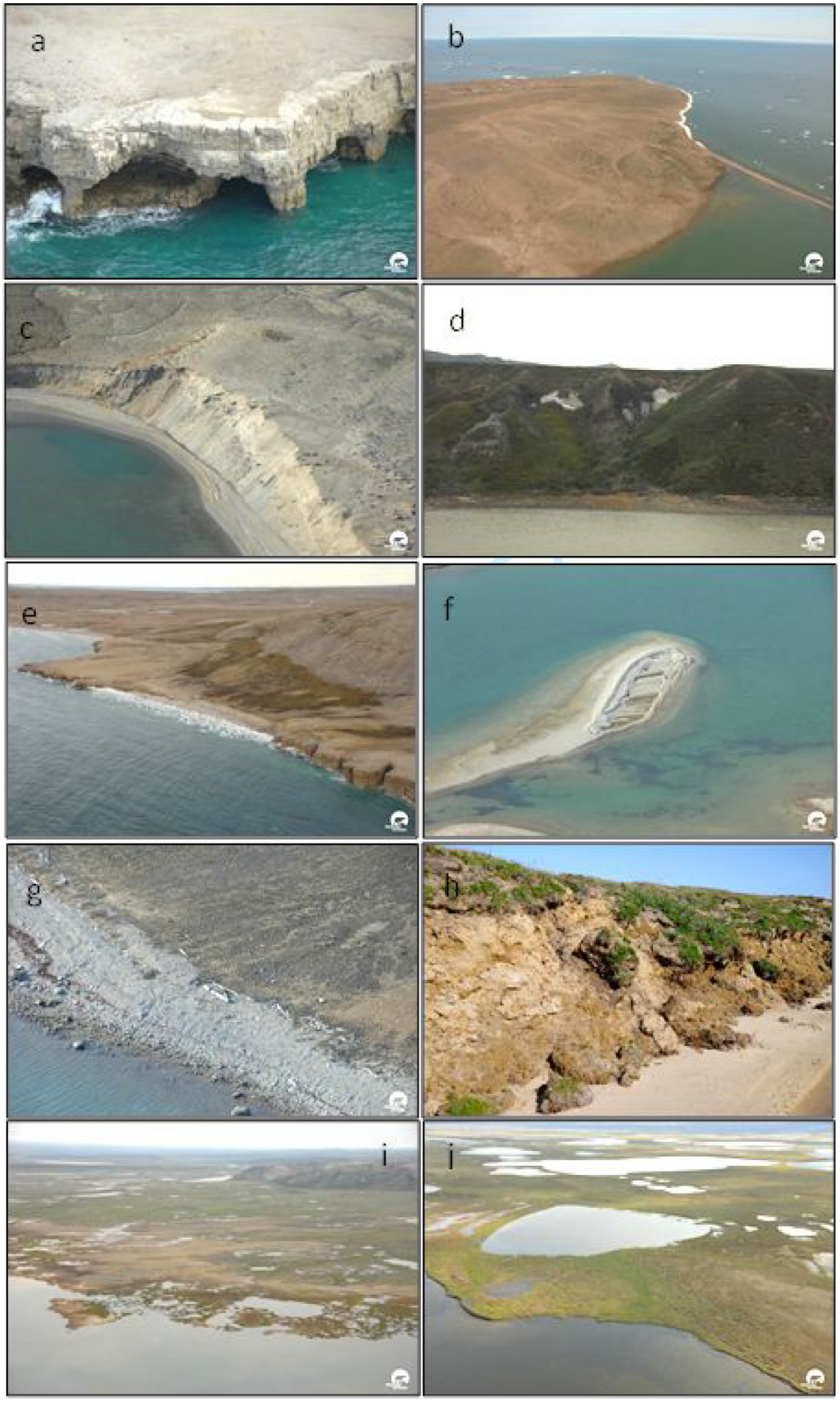

Table 3. Coastline changes analysis and DSAS parameters.

Coastal zone	Sector	Shorelines	Shoreline change rate uncertainty (m/yr)	Number of transects	Transect spacing (m)	Shoreline length (km)
Backshore	Eastern Parry Peninsula	1965–2020	0.05	5348	40	214
	Argo Bay–Paulatuk	1965–1993	0.10	398	40	15
		1993–2020	0.05	398	40	15
Foreshore	Eastern Parry Peninsula	1965–2020	0.05	7862	40	314
	Argo Bay–Paulatuk	1965–1993	0.10	707	40	28
		1993–2020	0.05	707	40	28

retreat as a proxy. Our calculations followed the method described by Lantuit et al. (2009), Obu et al. (2016), and Couture et al. (2018). The annual volumetric change was calculated using the cliff height, extracted from the ArcticDEM, the transect spacing, and the backshore retreat rate value for each transect following eq. 3

$$V_R = (1 - \varnothing) \times (h \times T_S \times R) \quad (3)$$

where V_R is the volume of removed sediments (m^3/yr), $\varnothing$ is the ground ice abundance (%) extracted from ground ice map of Canada (O'Neill et al. 2019), h is the cliff height (m), T_S is the transect spacing (m), and R is the shoreline retreat rate (m/yr). The ground ice abundance was extracted from the ground ice map of Canada (O'Neill et al. 2019), which provides an estimation of the volumetric percentage of excess ice in the top 5 m of permafrost (O'Neill et al. 2019). The volume of ground ice was accounted in the estimation of sediment volume release (eq. 3).

The SOCC grid from the Northern Circumpolar Soil Carbon Database provides information on the storage of permafrost SOC in the top 1 m of the soil and is based on pedon data (Hugelius et al. 2013). The annual SOC fluxes per meter of coast (kg C/m/yr) were estimated by multiplying the SOCC from the Northern Circumpolar Soil Carbon Database (Hugelius et al. 2013) with the shoreline retreat rates. Since this approach is based on the SOCC of the top 100 cm of the soil, it may underestimate the real SOCC released by the retreat of the total cliff face. However, most of the SOC is concentrated in the top soil and hence most of the global SOC estimates are based on it (Tarnocai et al. 2003; Hugelius et al. 2013).

Automatic satellite imagery-based shoreline extraction techniques use the sea to land contact as a proxy (Pardo-Pascual et al. 2012; Philipp et al. 2022). Therefore, regional shoreline change rates based on automatically delineated shorelines use the waterline, which may generate differences when compared with values obtained using the cliff-top, which is a more accurate proxy for volume estimates. To assess these differences, we compare the results of calculating sediment volume and SOC release using the cliff-top and waterline as proxies.

4. Results

4.1. Uncertainty evaluation

The evaluation of the shoreline change rate uncertainty shows values between 0.05 and 0.1 m/yr, revealing a particularly good quality in the assessment (Table 3). The lowest values were found in the analysis of the period from 1965 to 1993 for the Argo Bay–Paulatuk sector. This arises because of the lower resolution of the aerial imagery together with the shorter time span.

4.2. Backshore and foreshore characterization

The eastern coast of Parry Peninsula is characterized by two main distinct lithological units following the underlying geological composition (Fig. 1): an unconsolidated coast made of Cenozoic morainal deposits (Fig. 2A) and a coast of Paleozoic sedimentary carbonate rocks (Fig. 2B). Figure 5 shows the main landform types present along the coast, which are described in Table 2.

The backshore classification reveals that rocky coasts represent 60% of the total coast and occur mainly in the northern half of the study area (Fig. 6*a*). This sector, from Cape Parry to Clapperton Island, shows a very indented coast composed of Proterozoic dolostone forming numerous inlets and rocky headlands with spits separating sheltered coves (Fig. 5*b*). The high areas are rocky cliffs up to 20 m, where erosion created localized notches, arches, and pinnacles (Kerr 1994; Figs. 2B and 5*e*). Some 16 rocky islands are concentrated from Cape Parry to Clapperton Island, which is the largest, measuring c. 4.7 km × 2.7 km.

The low unconsolidated coastal stretches off the south of the study area in the Argo Bay to Paulatuk sector reappear at the latitude of Clapperton Island and Bennett Point for about 15 km. These two sections of unconsolidated materials show the same orientation and are exposed to the north-northeast (Figs. 1 and 5*c*). The unconsolidated sections present more linear coasts and are cut by rivers draining from thermokarst lakes, which can form large mouths or deltaic formations, such as the Hornaday river delta. Argo Bay is the largest bay inserted in the southwest and is the result of the flooding by the sea of an ancient lake (Harper 1990; Manson et al. 2005). Long spits of mixed sediments (primarily sand) partially close off the coastal bays or are anchored to the headlands (Fig. 5*g*).

Fig. 6. Morphological coastal classification of eastern Parry Peninsula: (*a*) backshore morphology and (*b*) foreshore morphology (ECCC 2017). Base map: © Esri. Projection: WGS 84/UTM zone 10.

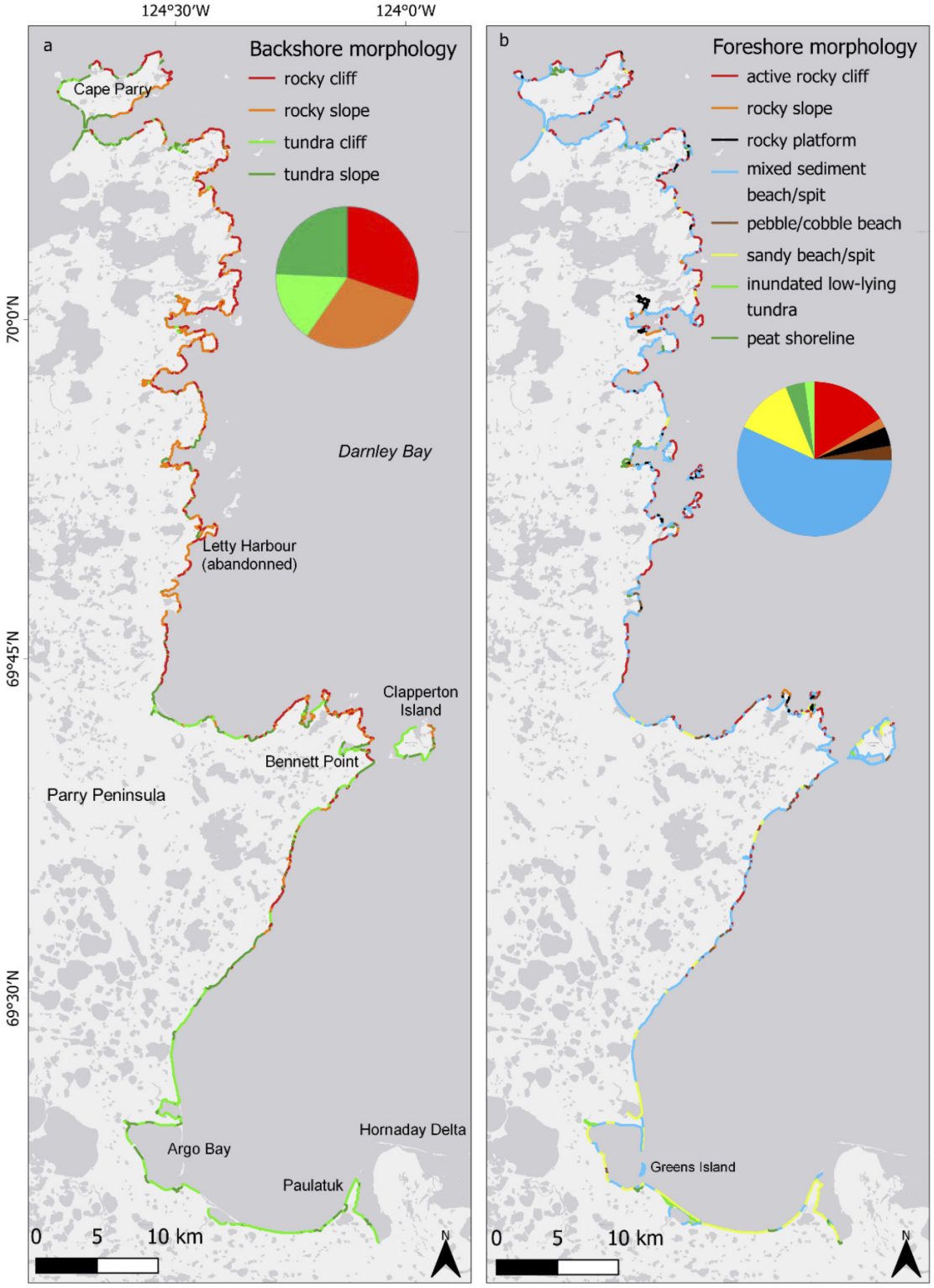

The foreshore classification reveals that mobile sedimentary features are fronting most of the backshore as sandy strips of mixed sediments of variable width (Figs. 5*c* and 5*h*) representing 71% of the coast (Fig. 6*b*). Sandy and gravel features are remobilized during the summer by waves and alongshore drift currents to form spits, tombolo, barrier beaches, and ridged beaches connected to the headlands showing the littoral drift orientation (Fig. 5*g*). In Cape Parry, numerous spits separate sheltered coves. Active rocky coasts are also present in the northern portion and represent 22%

Table 4. Summary statistics of shoreline change rates by coastal classification classes.

	Classes	Coverage km (%)	Mean retreat rate (m/yr)	Erosion %	Stable %	Accretion %	Max. retreat rate (m/yr)	Median
Backshore	Active rocky cliff	58 (18)	0.08	21	79	0	1.0	0.0
	Rocky cliff	39 (12)	0.09	26	74	0	0.8	0.05
	Rocky slope	91 (29)	0.10	28	72	0	0.13	0.05
	Tundra cliff	49 (16)	0.18	42	58	0	2.4	0.08
	Tundra slope	79 (24)	0.14	37	63	0	1.8	0.06
	Total	317	0.12	32	68	0	2.4	0.08
Foreshore	Active rocky cliff	59 (16)	0.08	43	46	0	0.2	0.08
	Rocky slope	7 (2)	0.09	39	53	0	1.05	0.07
	Rocky platform	15 (4)	0.10	36	57	0	0.2	0.07
	Pebble/cobble beach	12 (3)	0.18	58	34	8	1.22	0.13
	Mixed sediment beach	188 (49)	0.12	49	41	10	2.3	−0.10
	Sandy beach	47 (12)	0.28	55	35	11	2.83	0.13
	Mixed sediment spits	28 (7)	0.2	44	35	20	5.1	−0.05
	Peat shore	16 (4)	0.23	47	38	15	2.21	0.09
	Inundated low-lying tundra	8 (2)	0.19	51	24	24	0.48	0.11
	Total	380	0.16	48	41	14	5.1	0.10

of the coast (Table 4). Low-lying coasts such as peat shorelines and inundated low-lying tundra sectors represent only 6% of the coast and are located at the bottom of thermokarst basins and inlets.

4.3. Shoreline change analysis

4.3.1. Shoreline changes from 1965 to 2020

The results show differences between the backshore and foreshore retreat rates (Fig. 7). The overall mean retreat rate is 0.12 ± 0.05 m/yr for the backshore zone and 0.16 ± 0.05 m/yr for the foreshore zone. These values express an overall slowly retreating shoreline, with a greater variability of changes along the foreshore zone, while the backshore zone remains more stable. The foreshore zone is intrinsically more dynamic and tends to show both more erosion and accretion, because of its dominant composition of unconsolidated deposits, such as beaches or sand spits. Coasts showing change rates between −0.1 and 0.1 m/yr were classified as stable considering the highest shoreline change rate uncertainty, as shown in Table 3.

The analysis of the backshore zone reveals that 32% of the shoreline is undergoing retreat, while the rest is stable (Table 4). As expected, erosion rates are depending on the coastal material shown by the geology in Fig. 1. The Paleozoic sedimentary rocky coast is stable, while the morainal deposits coast is eroding at a mean rate of 0.2 m/yr. High erosion rates are located along four main locations of unconsolidated morainal coast: a section of 3 km along the western coast of Paulatuk shows erosion up 0.6 m/yr (Fig. 8*a*), a 2 km section at the south of Argo Bay shows mean retreat of 0.6 m/yr with maximum retreat of 1 m/yr (Fig. 8*b*), and two sections of 1 km located at the north Bennett Point and the south of Clapperton Island retreat at a mean rate of 0.8 m/yr with respective maximum retreat up to 1 and 1.4 m/yr. (Figs. 8*c* and 8*d*, Figs. 9A and 9B). These four sectors are exposing medium to high unconsolidated cliffs and are sometimes backed by tundra polygons. Together they are retreating at a mean rate of 0.55 m/yr.

The foreshore zone analysis shows that 48% of the shoreline is retreating, 10% is aggrading, and the rest remains stable. Again, a clear difference occurs in retreat rates between the unconsolidated and consolidated sectors of the coast (Fig. 7B). The foreshore zone is showing a larger range of shoreline change, with accretion up to 2.6 m/yr in large mixed sediment spit anchored in rocky headlands (Fig. 9C) and retreat up to 5.1 m/yr north of Greens Island (Fig. 9D).

Erosion along the foreshore zone is not necessarily correlative of erosion in the backshore zone of the same coastal section. Large parts of the backshore show stable cliffs, while the foreshore zone is eroding. An example is the sector with mixed sediment beaches halfway between Bennett Point and Argo Bay (Fig. 7). However, along fast retreating unconsolidated sectors, generally a simultaneous retreat of both coastal zones occurs. That occurred at the western coast of Paulatuk Peninsula, at the sector south of Argo Bay and south of Clapperton Island (Figs. 7 and 8*d*).

4.3.2. Shoreline changes from Argo Bay to Paulatuk

The spatial variability of shoreline changes was analyzed from Argo Bay to Paulatuk Peninsula from 1965 to 1993 and from 1993 to 2020, for both coastal zones (Table 5; Figs. 10 and 11).

The foreshore zone analysis shows an overall small decrease of the total mean retreat rates from 0.12 ± 0.1 m/yr

Fig. 7. Long-term change rates along the eastern coast of Parry Peninsula: (A) backshore zone and (B) foreshore zone. The inset in panel (B) is the coastline change analysis for two periods. Base map: © Esri. Projection: WGS 84/UTM zone 10.

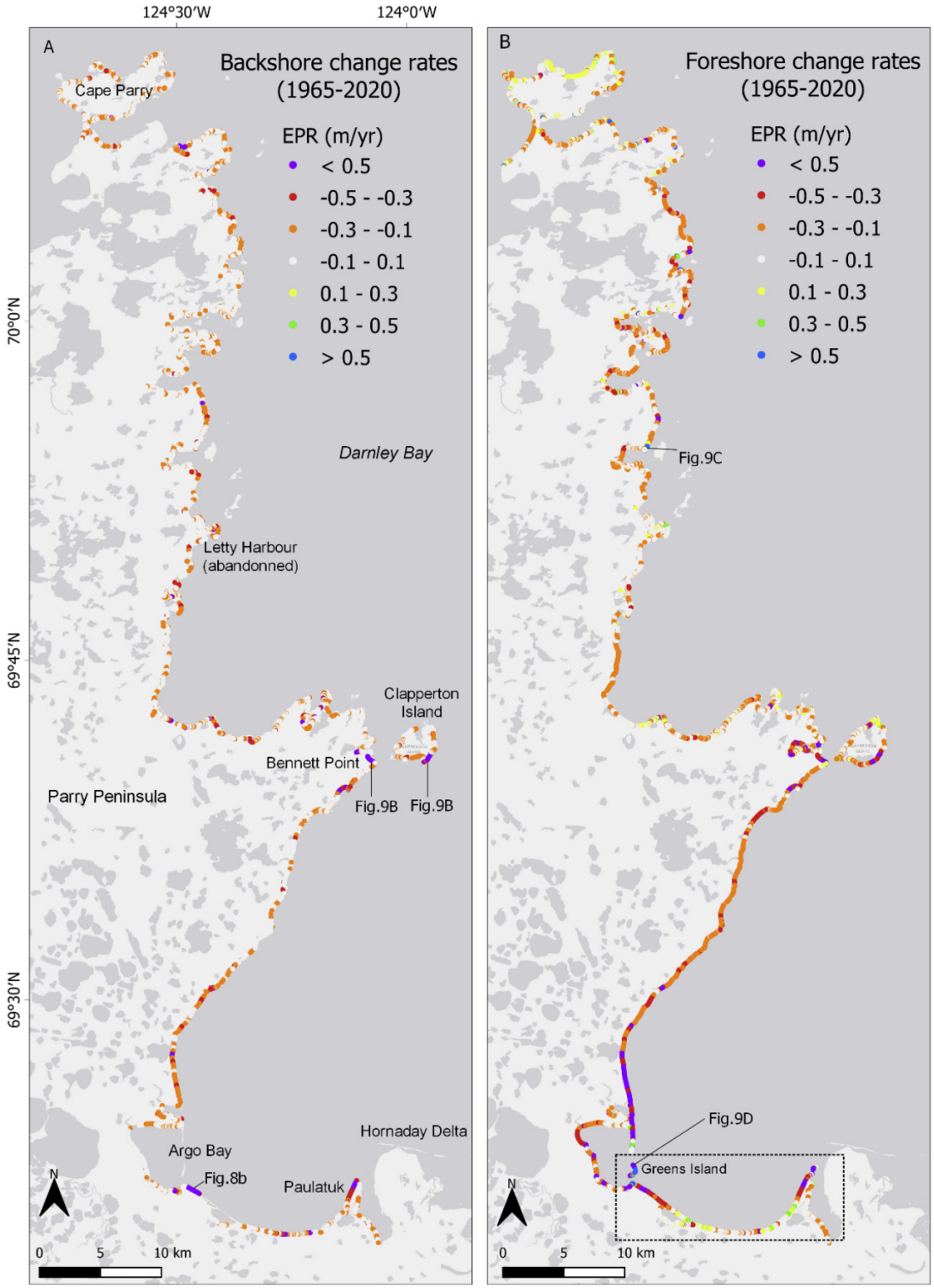

for 1965–1993 to 0.08 ± 0.05 m/yr for 1993–2020 (Table 5). High retreat rates occurred in the north of Greens Island during 1965–2020 with retreat up to 5.1 m/yr and accretion up to 1.8 m/yr (Figs. 8*d* and 10*a*). However, mean retreat rates varied from 0.10 ± 0.1 m/yr in 1965–1993 to 0.11± 0.05 m/yr in 1993–2020 and are not significantly different regarding uncertainty levels (Table 3). Retreat rates along the western coast of Paulatuk Peninsula varied from 0.14 ± 0.1 m/yr in 1965–1993 to 0.29 ± 0.05 m/yr in 1993–2020. The uncertainty level of ±0.1 m/yr in the first period does not allow to confirm

Fig. 8. Comparison between foreshore and backshore change rates along the four fastest eroding sectors in eastern Parry Peninsula showing simultaneous retreat of both zones at different pace.

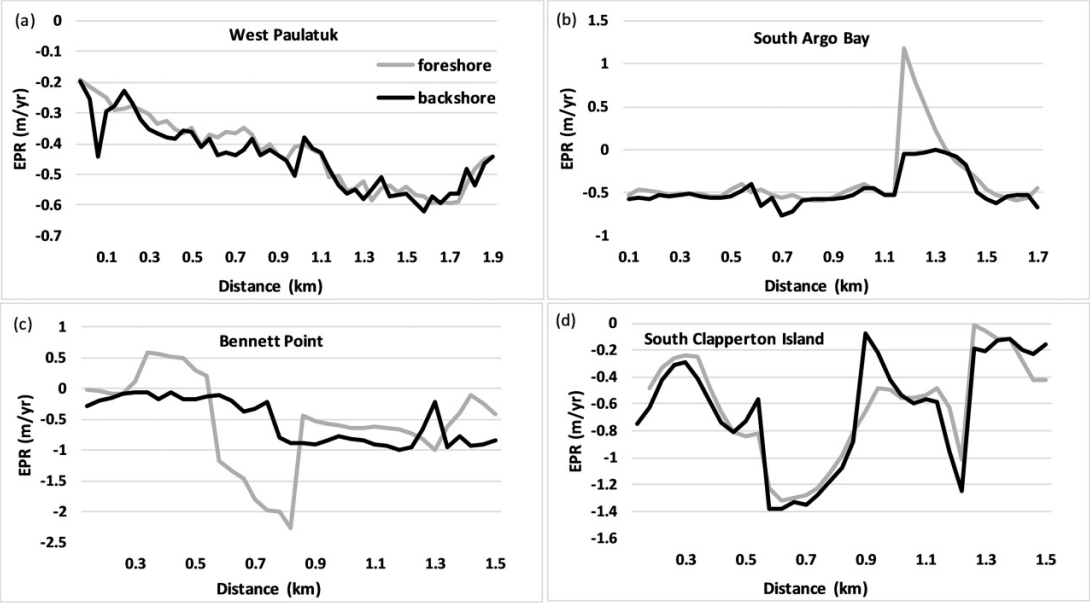

a statistically significant erosion increase of the foreshore zone.

The backshore zone analysis reveals higher mean retreat rates, varying from 0.17 ± 0.1 m/yr in 1965–1993 to 0.21 ± 0.05 m/yr in 1993–2020, which are not significant when considering the uncertainty levels (Tables 3 and 5).

However, retreat rates measured along the western tundra cliffs of Paulatuk, varying from 0.24 ± 0.1 m/yr in 1965–1993 to 0.47 ± 0.05 m/yr in 1993–2020, express a significant variation and confirm the recent increase in erosion of that area. The results also show that the eastern coast of Paulatuk remained stable (Figs. 10 and 11).

From Argo Bay to Paulatuk, the coastal morphology does not significantly influence the changes in rates. The highest mean retreat rates of 0.17 m/yr were measured along the tundra cliffs and mixed sediment beaches. The remaining accreting sectors between Greens Island and Paulatuk show overall low accretion rates and are characterized by sandy beaches. These results show that at the local scale, shoreline changes are significantly different and depend on the shoreline reference chosen. The foreshore analysis did not show a significant variation of the retreat rates at Paulatuk, while the backshore analysis confirmed increasing erosion of the tundra cliffs west of Paulatuk (Figs. 10 and 11).

4.3.3. Sediment volume and SOC release

The sediment volume and SOC release were estimated for the different coastal types using the cliff-top retreat rates for 1965–2020 (Table 6). The SOCC estimation extracted from the NCSCD grid ranges from 31 to 55 kg/m^3 over the studied coast. The region is characterized by medium ground ice abundance ranging between 10% and 20%, with high ground ice content in areas of thick and continuous till. The mean sediment volume loss was 20 m^3/m/yr with maximum rates up to 483 m^3/m/yr along tundra cliffs backed by ice-wedge polygon networks. The mean annual SOC release was 7 kg C/m of coast, with a maximum value of 134 kg C/m/yr along high tundra cliffs backed by ice-wedge polygons. Only 2% of the coast released more than 100 m^3/m/yr being these areas associated with medium (5–10 m) to high unconsolidated cliffs (>15 m). This 2% of coast shows a total sediment release from land to sea of 800 000 m^3/yr and 110 000 kg C/yr of SOC release.

Coastal sections with high ground ice content relate to unconsolidated tundra coasts and released higher sediment and SOC volumes. Backshore sections characterized by ice-wedge polygon networks and slumps released the highest mean volume of sediments of 42.2 m^3/yr and highest mean SOC fluxes of 11.3 kg C/yr, per meter of coast. At Bennett Point, a 1 km unconsolidated moraine section shows high retreat rates, ranging from 0.3 to 1.3 m/yr, showing a silty sediment plume until 200 m offshore in the Pléiades imagery (Fig. 9B). This single section showed a total sediment release of 56 000 m^3 and total SOC release of 36 000 kg/yr. Together, the four fastest retreating sites of the backshore zone contribute to an estimated total release of 270 000 m^3 of sediment and 190 000 kg of SOC to the nearshore zone per year.

The comparison between using either the foreshore or the backshore zone as proxies reveals that differences in shoreline change rates, sediment volume, and SOC estimates are statistically significant (Fig. 12). The analysis shows that for estimating sediment volume and SOC release at a regional scale, the use of the waterline tends to overestimate the results by, respectively, 20% and 22% (Table 7; Fig. 12). This overestimation is due to the general highest retreat rates obtained when measuring the waterline, instead of the cliff-top (Fig. 12), since this relates to spits and

Fig. 9. Examples of shoreline change rates for the backshore zone (A, B) and foreshore zone (C, D) with rates and historical shorelines. Panel (B) shows a sediment plume of silty sediments eroded from the adjacent tundra cliff to the coastal waters at Bennett Point. Base map: PLEIADES © CNES, 2020, distribution Airbus DS. The location of the images is shown in Fig. 7. Projection: WGS 84/UTM zone 10.

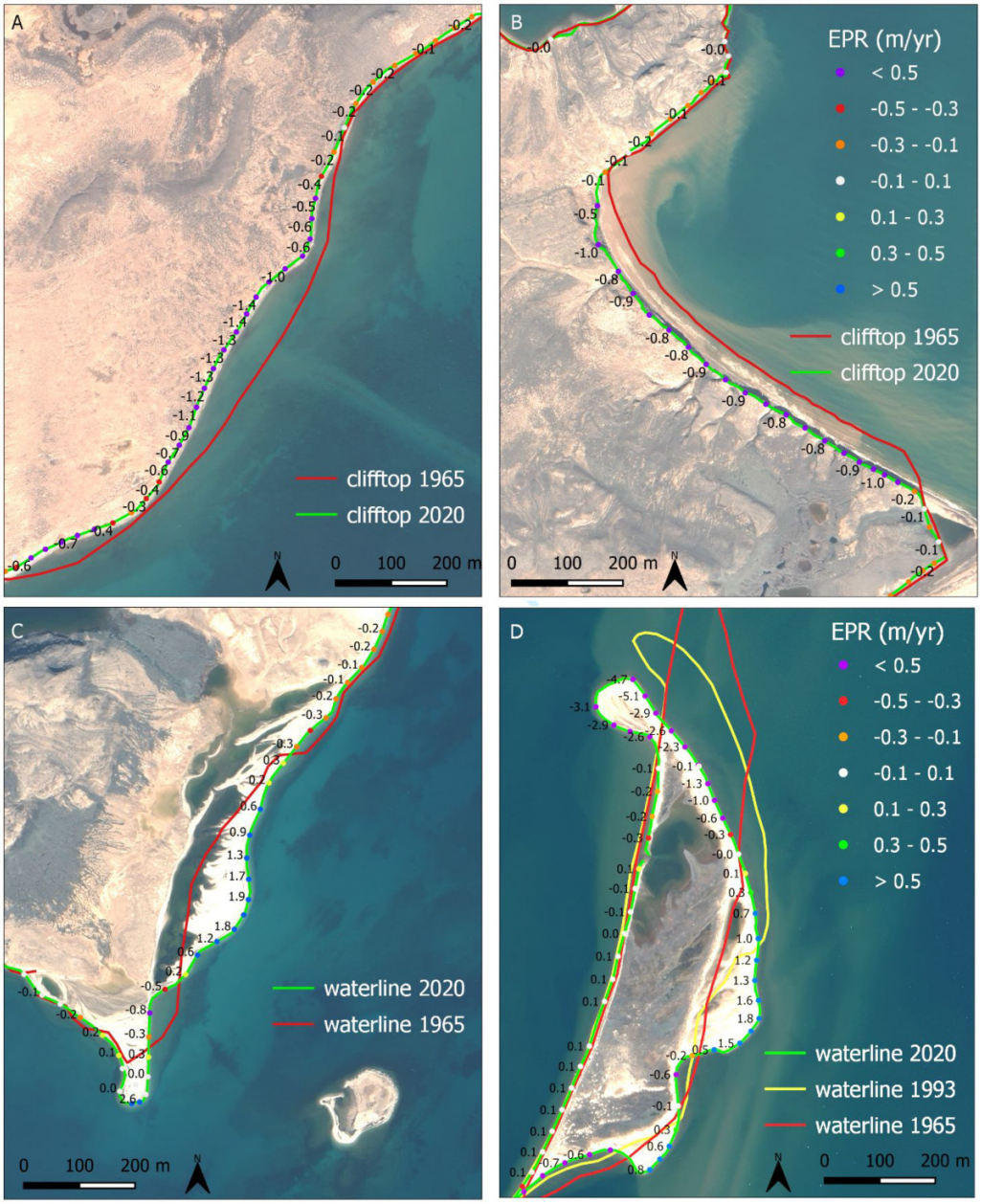

Table 5. Coastline change rates between 1965–1993 and 1993–2020 in function of the coastal morphology along the Argo Bay–Paulatuk section.

		Length (km)	Foreshore EPR 1965–1993	Foreshore EPR 1993–2020	Backshore EPR 1965–1993	Backshore EPR 1993–2020
Coastal morphology	Inundated low-lying tundra	2	0.03	−0.05	–	–
	Sandy beach	17	−0.12	−0.06	–	–
	Mixed sediment beach	8	−0.10	−0.17	–	–
	Tundra cliff	24	–	–	−0.17	−0.08
Sectors	Greens Island	2.4	−0.10	−0.11	–	–
	West Paulatuk	4.2	−0.14	−0.29	**−0.24**	**−0.47**
	East Paulatuk	3.2	−0.10	0.03	−0.05	−0.05
	Total	27	−0.12	−0.08	−0.17	−0.21

Fig. 10. Spatiotemporal variability of shoreline change rates between Argo Bay and Paulatuk between 1965–1993 and 1993–2020 for the foreshore and backshore zones.

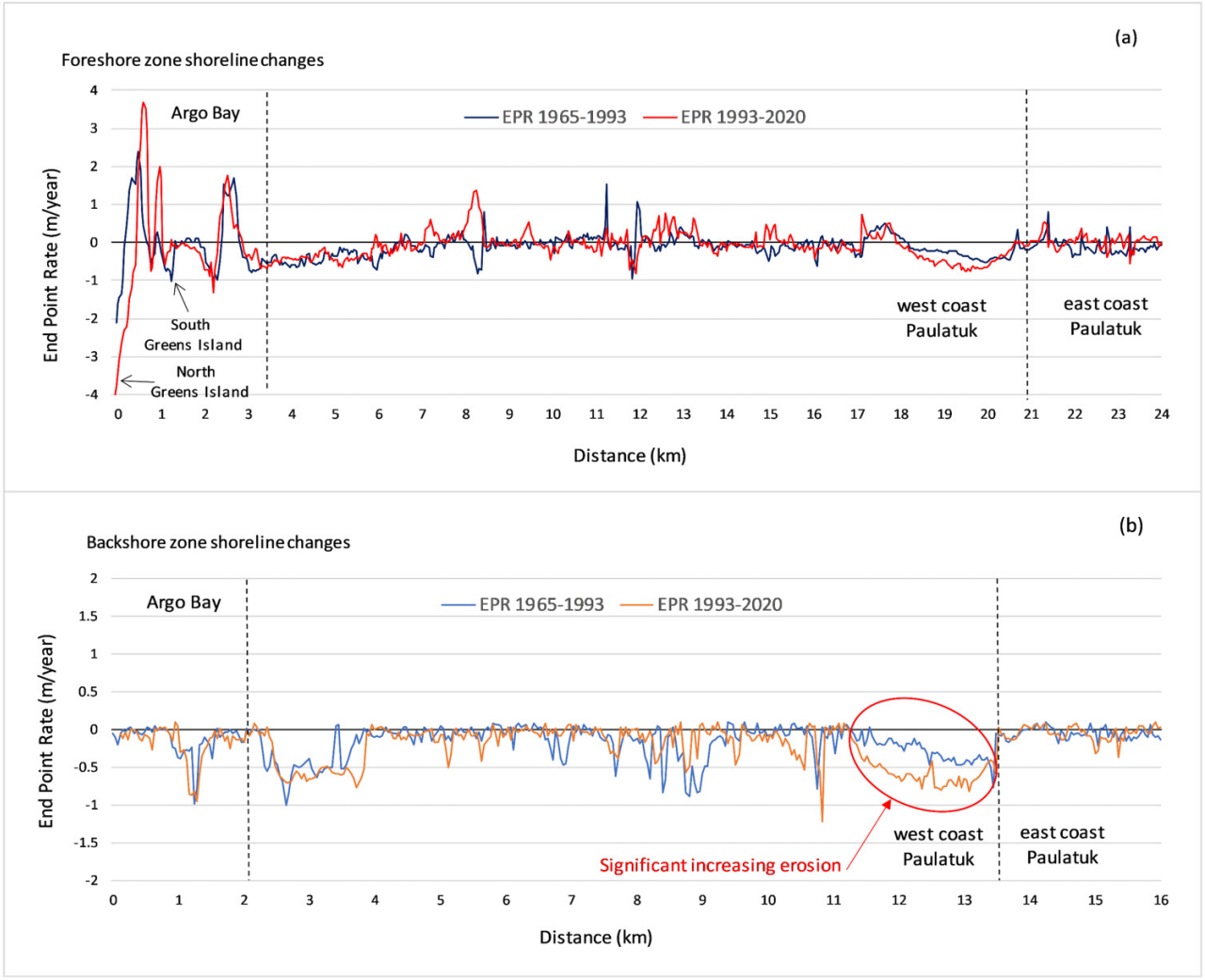

beaches that have no direct relation to cliff degradation in the backshore.

5. Discussion

5.1. Shoreline change rates

The general orientation of the coast, the duration of the sea ice season, the ground ice content, wave power, and local climate have been identified as driving factors of erosion on Arctic coasts (Gibbs et al. 2021; Irrgang et al. 2022). In eastern Parry Peninsula, the sediment remobilization seems to be slow due to the limited wave action. With the predominantly rocky composition and low ice content, the studied coast does not show high mobility and its change rates are typical of stable rocky coasts. Our study has revealed an overall slowly retreating coastline for both coastal zones, with variability in function of the type of material exposed. The indented profile of the northern rocky coastal sector seems to play a significant role in the reduction of the swell energy due to diffraction. However, volumetric loss was identified from cliff-top retreat in several sectors, but it may be due to thermal abrasion and thawing processes rather than wave impact. On the other hand, low-lying coastal landforms subject to flooding, overwash, or breaching are sparsely present along Parry Peninsula. These are often the cause of consequent shoreline retreat that can extend for hundreds of meters as in the case of the breached thermokarst lakes after the erosion of its seaward banks, creating bays as found along the Tuktoyaktuk Peninsula. Eastern Parry Peninsula presents some structures associated with former lakes but breaching has not been detected after a detailed analysis of the imagery between 1965 and 2020.

The mean retreat rates of 0.12 m/yr for the backshore zone and 0.16 m/yr for the foreshore are very low when compared with other long-term studies on unconsolidated coasts of the Beaufort Sea, where Irrgang et al. (2018) report an average retreat rate of 0.7 m/yr along the Yukon coastal plain or the 2.2 m/yr observed by Cunliffe et al. (2019) on Herschel Island. Indeed, changes occurring on those ice-rich unconsolidated

Fig. 11. Backshore change rates in Paulatuk during the 1965–1993 (A) and 1993–2020 (B) time periods. Base map: PLEIADES © CNES, 2020, distribution Airbus DS. Projection: WGS 84/UTM zone 10.

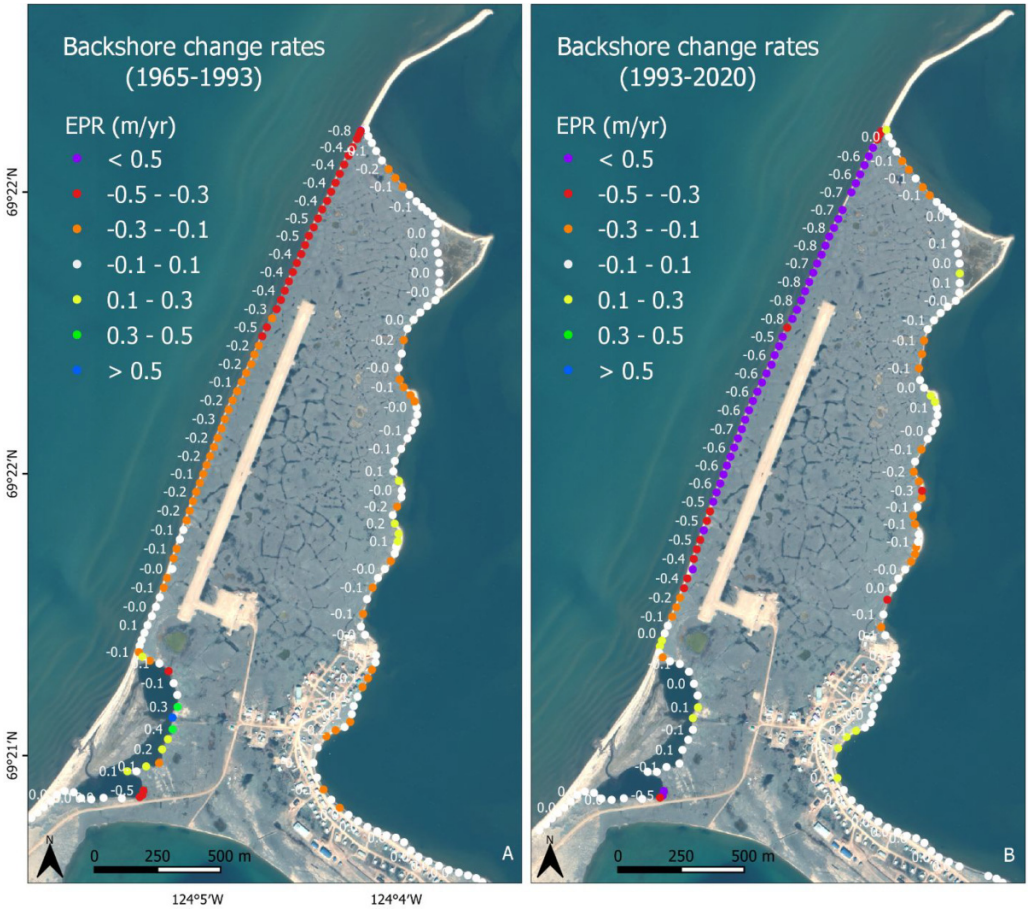

Table 6. Estimated sediment volume and soil organic carbon release in function of the backshore coastal types.

Coastal types	Erosion rates (m/yr)	Cliff height (m)	SOCC (kg/m^3)	Ground ice abundance (%)	Sediment volume flux (m^3/m/yr)	Total sediment volume flux(m^3/yr·10^3)	SOC flux(kg C/m/yr)	Total SOC flux(kg C/yr·10^3)
Active rocky cliff	0.08 ± 0.05	6.7	49	10–20	17	690	4.6	187
Rocky cliff	0.09 ± 0.05	7.5	54	10–20	22.4	458	5.1	104
Rocky slope	0.10 ± 0.05	3.2	55	10–20	10.5	569	5.8	317
Tundra slope	0.14 ± 0.05	3.4	54	20–30	13.2	570	7.6	330
Tundra cliff	0.18 ± 0.05	6.9	54	20–30	33.4	1854	9.1	497
Tundra polygons and slumps	0.22 ± 0.05	6.8	52	20–30	42.2	835	11.3	225
Mean	0.13 ± 0.05	5.3	54	10–20	19	–	6.7	–
Min.	0	0	31	0	0	–	0	–
Max.	2.4 ± 0.05	35	55	30	483	–	134	–
Total	–	–	–	–	–	4976	–	1660

coasts are governed by permafrost thawing and wave impact, resulting in rapid mass movements, such as thaw slumps or block failures. The wave power on ice-rich unconsolidated coast of the Beaufort Sea (Tuktoyaktuk, Yukon coast, Mackenzie Delta) is more significant due to their orientation and exposure to a larger fetch area (Manson et al. 2005; Berry et al. 2021; Gibbs et al. 2021). The ground ice content of those coasts is also much higher and coastal retreat can exceed

Fig. 12. Comparative box plots of shoreline change rates, sediment volume, and SOC release rates between foreshore and backshore analyses, showing statistical difference at 0.05 significance level from *t* test. The center line represents the median and extreme values have been removed.

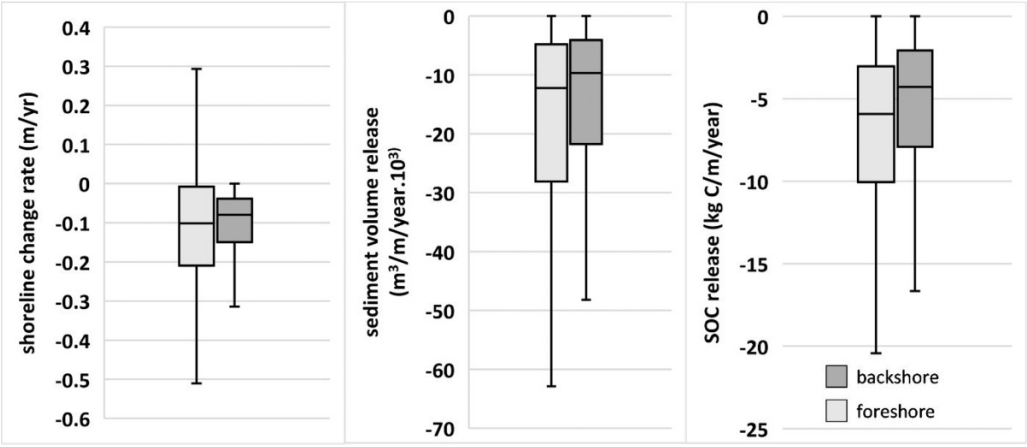

Table 7. Sediment volume and SOC fluxes compared by coastal zone.

	Total shoreline	Time period	Erosion rate (m/yr)	Mean sediment volume flux(m^3/m/yr)	Total sediment volume flux(m^3/yr·10^3)	Mean SOC flux(kg C/m/yr)	Total SOC flux(kg C/yr·10^3)
Backshore	341	1965–2020	0.13	19	4976	6.7	1660
Foreshore	353	1965–2020	0.20	23	5966	8.4	1941
Percentage difference	–	–	–	19%	20%	22%	17%

Note: The backshore zone is defined using the cliff-top line and the foreshore zone using the waterline.

20 m/yr in some areas or massive ground ice (Lantuit and Pollard 2008; Obu et al. 2017; Lim et al. 2020; Berry et al. 2021). Our results highlight the susceptibility of unconsolidated sediment to storms and thawing, as shown in fast retreating sectors along tundra cliffs with 2.4 m/yr and mixed sediment spits with 5.1 m/yr and with significant increasing erosion in the Paulatuk Peninsula.

Sankar et al. (2019) studied shoreline changes in Paulatuk Peninsula between 1984 and 2016 and revealed an increase of the erosion rates in Paulatuk in recent decades (2006–2016) in response to recent warming, longer ice-free season, and increasing storminess. They report a mean rate of change of 0.11 m/yr along the western coast and −0.12 m/yr along the eastern coast from 1984 to 2016. From 2006 to 2016, the western coast showed retreat rates of 0.24 m/yr and the eastern coast showed 0.34 m/yr. Our results show that erosion dominated the western coast of Paulatuk for both long-term and short-term analyses, with mean cliff-top retreat rates of 0.47 m/yr from 1993 to 2020, confirming the increase of erosion in recent decades. However, we found that the eastern coast remained mostly stable. The difference in average retreat rates between the western and eastern coasts of Paulatuk can be explained by the coastal orientation and a greater exposure to swells on the western side, while the eastern coast is sheltered by a 3 km long sandy spit in the north and exposed to a smaller fetch area (Fig. 11).

The difference in values compared with those of Sankar et al. (2019) can be explained by the different resolution of the imagery, the different periods of analysis, and the shoreline extraction method. Automatic shoreline extraction methods for Landsat images are sensitive to shadowing issues and thresholding and band-ratio methods for edge detection result in higher shoreline position errors, than with manual shoreline digitizing from higher resolution imagery (Pardo-Pascual et al. 2012). The southward sediment migration in Greens Island and the increasing retreat rates in the western coast of Paulatuk may be the result of increasing storminess within Darnley Bay in recent decades but could also be related to increase in air temperatures leading to thawing permafrost (Sankar et al. 2019; Berry et al. 2021).

5.2. Sediment volume and SOC fluxes

Our analysis shows that low erosion on medium to high unconsolidated cliffs can release sediment volumes up to 3300 m^3/yr·10^3 (Table 6). However, the method we have used, based on planimetric data combined with cliff height, generally underestimates volume release when compared with a DEM subtraction method (Obu et al. 2016). Moreover, the estimation of SOC fluxes is based on the SOCC of the first 100 cm of soil depth, neglecting the total amount of SOC stored within the total cliff face. Along the Yukon coastal plain, on average the top meter contains 43.2% of the SOC of the total soil column with SOCC ranging from 30 to 55 kg C/m^3 (Couture et al. 2018). Other studies indicate that in Arctic coasts, mean

annual fluxes range from 73 kg C/m in the Alaskan Beaufort coast (Ping et al. 2011) to 375 kg C/m at the Laptev and East Siberian Seas (Rachold et al. 2004). The Yukon coastal plain shows intermediate rates of 132 kg C/m (Couture et al. 2018). The regional differences are explained by cliff height, ground ice volume, and SOCC and retreat rates variability. The Laptev and East Siberian Seas contribute for three quarters of the pan-Arctic SOC losses, due to the very high erosion rates, very high ground ice content (80%), and very high SOCC (Nielsen et al. 2022). The Beaufort Sea coast presents mean retreat rates of 1.1 m/yr and an average ground ice content of 28.5% (Overduin et al. 2014). Retrogressive thaw slumps and block failures are typical mass wasting processes, particularly present on ice-rich coasts such as the Yukon coastal plain, Richards and Herschel Islands. The eastern Parry Peninsula shoreline does not show such evidence of thermo-erosion and high SOC fluxes, since retreat rates are low as well as the ground ice content due to the dominant rocky lithology. However, we identified four sites showing high sediment and SOC release, which potentially may show potential impacts on the nearshore zone and habitats: the western coast of Paulatuk Peninsula, a 1 km section at the southern limit of Argo Bay, the northern sector of Bennett Point (Fig. 9B), and a section south of Clapperton (Fig. 9A). Coastal erosion was found to be an important contributor to organic carbon and contaminant release in coastal waters (St Pierre et al. 2018; Jones et al. 2020), potentially impacting nearshore marine ecosystems. The increase of terrestrial OC transfers into the coastal waters will change the nutrient budget and impact the coastal water biochemistry, influencing the acidification of coastal waters and potentially altering the marine primary production, affecting marine food webs, fish and marine mammal's stocks and distributions (Mann et al. 2022). Further investigation for the environmental assessment of the potential impacts on the AN-MPA should be conducted at these sites.

5.3. Impacts of proxy usage

The application of automatic coastal delineation algorithms using remote sensing imagery is usually based on the detection of the waterline through spectral indices, pixel segmentation, and various classification techniques, with recent examples being CoastSat, Waterdetect, or XGBoost (Vos et al. 2019; Aryal et al. 2021; Cordeiro et al. 2021). Our comparative analysis has shown that the shoreline changes and volume transfer estimates can be very different depending on the shoreline proxy used—backshore versus foreshore. Eamer et al. (2021) draw similar conclusions in a comparative analysis of changes between waterline and vegetation marks, finding poor correlation between the proxies and differences in coastline evolution.

Furthermore, to more accurately calculate sediment and SOC release associated with coastal erosion, it is important to focus on the retreat of the cliffs, which are the most important source of material associated with coastal erosion (Pfalz, 2017; Grotheer et al. 2020). To assess the differences of applying both methods, we further calculated the sediment volume and SOC release using the waterline as a shoreline proxy. The results show that the use of the waterline and associated retreat rates significantly overestimate sediment volume and SOC fluxes when compared with the use of the cliff-top (Table 7; Fig. 12). The use of the waterline characterizes the changes occurring within the foreshore zone, which was predominantly characterized by mixed sediment beaches and should show much lower SOC fluxes than those derived from the backshore zone. Our results, which are valid only for the study area, suggest that the use of the waterline or wet/dry line as shoreline proxy can result in an error of +22% for SOC flux estimations. This bias needs to be considered for regional-scale shoreline change analysis using satellite data such as Landsat or Sentinel-2 imagery with automatic shoreline extraction methods.

6. Conclusions

High-resolution multispectral scenes from the Pléiades satellite of 2020 and historical aerial imagery from 1965 allowed to describe and characterize the shoreline changes in the eastern coast of the Parry Peninsula. In the area from Argo Bay to Paulatuk, the analysis of aerial imagery from 1993 provided further insight into the evolution of shoreline change rates. This study highlights the variability of the shoreline in this ecologically important area within the AN-MPA. Our main conclusions are as follows:

(a) The coastal morphology of the backshore zone of east Parry Peninsula is dominated by consolidated coasts in the north and unconsolidated coasts with higher ground ice content in the south. The foreshore zone is characterized by extensive depositional landforms reworked by waves and currents during the ice-free season, forming beaches and spits.

(b) The shoreline change rates reveal a low retreating shoreline when compared with other regions of the Arctic. However, spatial variability occurs as a function of the coastal zones and their morphology. From 1965 to 2020, the backshore retreated at a rate of 0.12 m/yr with higher rates along tundra cliffs. The foreshore retreated at a rate of 0.16 m/yr showing higher erosion rates along spits and beaches, of up to 5 m/yr. The analysis of the area from Argo Bay to Paulatuk comparing 1965–1993 and 1993–2020 change rates shows that blufftop retreat rates have doubled along the exposed western coast of Paulatuk.

(c) High erosion rates are concentrated around four main locations classified as tundra cliffs in thick moraine deposits: erosion rates of up to 1.4 m/yr south of Clapperton Island, 1 m/yr at Bennett Point, 1 m/yr south of Argo Bay, and 0.8 m/yr at the western coast of Paulatuk. The coast has eroded up to 33 m at west Paulatuk since 1965. These four sites contributed to an estimated total release of 270 000 m^3/yr of sediment and 190 000 kg/yr of SOC to the nearshore zone.

(d) Across the study area, the total estimated sediment volume release was about 5000 $m^3/yr \cdot 10^3$, with mean an-

nual sediment volume transfer from land to the ocean of about 20 m^3/m/yr. The total SOC flux was 1660 kg C/yr·10^3 with an average of about 7 kg C/m/yr. Tundra cliffs with ice-wedge polygons released the highest amounts of organic carbon.

The detailed classification of the coast and the analysis of the foreshore and backshore zones allowed to provide new insight into their dynamics in an area where studies were lacking, probably due to the prevailing rocky nature of the cliffs and scarce erosion. We have shown that significant differences are found when estimating sediment and SOC fluxes associated with erosion, if the waterline or the cliff-top line is used. These differences account in eastern Darnley Bay for an overestimation of mean sediment fluxes of c. 19% and of mean SOC fluxes of up to 22%. These differences are high and can have severe impacts upon regional estimations in studies that use the waterline as a proxy for the shore. Hence, we recommend that automatic shoreline delineation algorithms focus on the best proxy for sediment transfer, which may not be the waterline in many cases, especially where sea does not directly contact with the cliff-base. In this case, the cliff-top (or the cliff-base) should be used instead.

Acknowledgements

This project is made possible by funding from the Natural Resources Canada, Climate Change Geoscience Program, Crown-Indigenous Relations and Northern Affairs Canada (CIRNAC) through the Beaufort Sea Regional Strategic Environment and Research Assessment (BRSEA) and by the European Union's Horizon 2020 Research and Innovation Program under grant agreement No. 773421 (Project NUNATARYUK). Pléiades imagery was acquired through the ISIS Pléiades Program in connection with the WMO Polar Space Task Group. This work falls under the Northwest Territories Scientific Research permit (#16490), and support from the community of Paulatuk via consultation with the Paulatuk Hunters and Trappers committee in August 2019 and again in March 2020. Their advice and questions provided the basis of the research. We sincerely thank Mr. Marc Dubrule and CanFly Drones, Edmonton, for the consulting and support concerning RPAS operations in Canada.

Article information

History dates

Received: 8 June 2022
Accepted: 3 December 2022
Accepted manuscript online: 2 February 2023
Version of record online: 2 March 2023

Copyright

Data availability

Data generated or analyzed during this study are available in the (Zenodo) repository (https://doi.org/10.5281/zenodo.7572256).

Author information

Author ORCIDs

Rodrigue Tanguy https://orcid.org/0000-0002-8575-9061

Author contributions

Conceptualization: RT, DW, GP, GV
Formal analysis: RT, DW, GV
Investigation: RT, DW, GP, GV
Methodology: RT, DW, GP, GV
Resources: DW, GV
Supervision: DW, GP, GV
Validation: RT
Visualization: RT
Writing – original draft: RT
Writing – review & editing: RT, DW, GP, GV

Competing interests

The authors declare that there are no competing interests.

References

Aryal, B., Escarzaga, S.M., Vargas Zesati, S.A., Velez-Reyes, M., Fuentes, O., and Tweedie, C. 2021. Semi-automated semantic segmentation of Arctic shorelines using very high-resolution airborne imagery, spectral indices and weakly supervised machine learning approaches. Remote Sensing, **13**: 4572. doi:10.3390/rs13224572.

Atkinson, D.E., Forbes, D.L., and James, T.S. 2016. Canada's marine coasts in a changing climate. *Edited by* D.S. Lemmen, F.J. Warren, T.S. James and C.S.L. Mercer Clarke. Government of Canada, Ottawa. pp. 27–68.

Berry, H.B., Whalen, D., and Lim, M. 2021. Long-term ice-rich permafrost coast sensitivity to air temperatures and storm influence: lessons from Pullen Island, Northwest Territories Canada. Arctic Science, **7**(4): 723–745. doi:10.1139/as-2020-0003.

Cordeiro, M.C., Martinez, J.M., and Peña-Luque, S. 2021. Automatic water detection from multidimensional hierarchical clustering for Sentinel-2 images and a comparison with Level 2A processors. Remote Sensing of Environment, **253**: 112209. doi:10.1016/j.rse.2020.112209.

Couture, N.J., Fritz, M., Irrgang, A., Pollard, W., and Lantuit, H. 2018. Coastal erosion of permafrost soils along the Yukon coastal plain and fluxes of organic carbon to the Canadian Beaufort Sea. Journal of Geophysical Research: Biogeosciences, **123**: 406–422. doi:10.1002/2017JG004166.

Cunliffe, A.M., Tanski, G., Radosavljevic, B., Palmer, W.F., Sachs, T., Lantuit, H., et al. 2019. Rapid retreat of permafrost coastline observed with aerial drone photogrammetry. The Cryosphere, **13**: 1513–1528. doi:10.5194/tc-13-1513-2019.

Eamer, J.B., Didier, D., Kehler, D., Manning, I., Colville, D., Manson, G., et al. 2021. Multi-decadal coastal evolution of a North Atlantic shelf-edge vegetated sand island—Sable Island, Canada. Canadian Journal of Earth Sciences, **99**(999): 1–14. doi:10.1139/cjes-2020-0194.

Environment and Climate Change Canada. 2017. Northern Canada shoreline classification[shapefile]. Available from https://open.canada.ca/data/en/dataset/1c61d457-4d03-4f3a-9005-9aabb5a201bb.

Environment Canada. 2014. Paulatuk A and Cape Parry A, Canadian climate normals 1981–2010. from the original: (CSV (3069 KB)).

Environment Canada. 2015. Beaufort regional coastal sensitivity atlas. Government of Canada, Gatineau, Québec.

Fast, H., Mathias, J., and Banias, O. 2001. Directions toward marine conservation in Canada's Western Arctic. Ocean and Coastal Management, **44**(3–4): 183–205. doi:10.1016/S0964-5691(00)00074-0.

Fequet, D., Haché, L., McCourt, S., Langlois, D., Dicaire, C., Premont, B., et al. 2011. Sea ice climatic atlas for the northern Canadian waters 1981–2010. Environment Canada. Available from https://www.canada.ca/en/environment-climate-change/services/ice-forecasts-observations/publications/sea-climatic-atlas-northern-waters-1981-2010.html.

Galley, R.J., Key, E.L., Barber, D.G., Hwang, B., and Ehn, J.K. 2008. Spatial and temporal variability of sea ice in the southern Beaufort Sea and Amundsen Gulf: 1980–2004. Journal of Geophysical Research, **113**: C5. doi:10.1029/2007JC004553.

Gibbs, A., Erikson, L., Jones, B., Richmond, B., and Engelstad, A. 2021. Seven decades of coastal change at Barter Island, Alaska: exploring the importance of waves and temperature on erosion of coastal permafrost bluffs. Remote Sensing, **13**(21): 4420. doi:10.3390/rs13214420.

Grotheer, H., Meyer, V., Riedel, T., Pfalz, G., Mathieu, L., Hefter, J., and Fritz, M. 2020. Burial and origin of permafrost-derived carbon in the nearshore zone of the southern Canadian Beaufort Sea. Geophysical Research Letters, **47**(3): e2019GL085897. doi:10.1029/2019GL085897.

Harper, J.R. 1990. Morphology of the Canadian Beaufort Sea coast. Marine Geology, **91**: 75–91. doi:10.1016/0025-3227(90)90134-6.

Hequette, A., and Barnes, P.W. 1990. Coastal retreat and shoreface profile variations in the Canadian Beaufort Sea. Marine Geology, **91**, (1–2): 113–1332. doi:10.1016/0025-3227(90)90136-8.

Himmelstoss, E.A., Henderson, R.E., Kratzmann, M.G., and Farris, A.S. 2018. Digital Coastline Analysis System (DSAS) version 5.0 user guide. U.S. Geological Survey, Open-File Report 2018–1179. doi:10.3133/ofr20181179.

Hugelius, G., Tarnocai, C., Broll, G., Canadell, J.G., Kuhry, P., and Swanson, D.K. 2013. The northern circumpolar soil carbon database: spatially distributed datasets of soil coverage and soil carbon storage in the northern permafrost regions. Earth System Science Data, **5**(1): 3–13. doi:10.5194/essd-5-3-2013.

IPCC. 2019. IPCC Special Report on the Ocean and Cryosphere in a Changing Climate. *Edited by* H.O. Portner, D.C. Roberts, V. Masson-Delmotte, P. Zhai, M. Tignor, E. Poloczanska, K. Mintenbeck, A. Alegria, M. Nicolai, A. Okem, J. Petzold, B. Rama and N.M. Weyer. In press.

Irrgang, A.M., Bendixen, M., Farquharson, L.M., Baranskaya, A.V., Erikson, L.H., Gibbs, A.E., et al. 2022. Drivers, dynamics and impacts of changing Arctic coasts. Nature Reviews Earth & Environment, **3**(1): 39–54. doi:10.1038/s43017-021-00232-1.

Irrgang, A.M., Lantuit, H., Manson, G.K., and Günther, F. 2018. Variability in rates of coastal change along the Yukon coast, 1951 to 2015. Journal of Geophysical Research: Earth Surface, **2005**: 779–800. doi:10.1002/2017JF004326.

Jones, B.M., Arp, C.D., Jorgenson, M.T., Hinkel, K.M., Schmutz, J.A., and Flint, P.L. 2009. Increase in the rate and uniformity of coastline erosion in Arctic Alaska. Geophysical Research Letters, **36**(3). doi:10.1029/2008GL036205.

Jones, B.M., Irrgang, A.M., Farquharson, L.M., Lantuit, H., Whalen, D., Ogorodov, S., et al. 2020. Arctic report card: update for 2020. The sustained transformation to a warmer, less frozen and biologically changed Arctic remains clear. Available from https://arctic.noaa.gov/Report-Card/Report-Card-2020/ArtMID/7975/ArticleID/904/Coastal-Permafrost-Erosion.

Kerr, D. 1994. Late Quaternary stratigraphy and depositional history of the Parry Peninsula-Perry River area, District of Mackenzie, Northwest Territories. Geological Survey of Canada, Ottawa.

Lantuit, H., and Pollard, W.H. 2008. Fifty years of coastal erosion and retrogressive thaw slump activity on Herschel Island, Southern Beaufort Sea, Yukon Territory, Canada. Geomorphology, **95**: 84–102. doi:10.1016/j.geomorph.2006.07.040.

Lantuit, H., Overduin, P.P., Couture, N., Wetterich, S., Are, F., Atkinson, D., et al. 2012. The Arctic Coastal Dynamics database. A new classification scheme and statistics on Arctic permafrost coastlines. Estuaries and Coasts, **35**(2): 383–400. doi:10.1007/s12237-010-9362-6.

Lantuit, H., Rachold, V., Pollard, W.H., Steenhuisen, F., Ødegård, R., and Hubberten, H.W. 2009. Towards a calculation of organic carbon release from erosion of Arctic coasts using non-fractal coastline datasets. Marine Geology, **257**(1): 1–10. doi:10.1016/j.margeo.2008.10.004.

Latour, P.B. 2008. Key migratory bird terrestrial habitat sites in the Northwest Territories and Nunavut.3rd ed. Canadian Wildlife Service, Ottawa, Ontario. ISBN: 9780662467205.

Lim, M., Whalen, D., Martin, J., and Mann, P.J. 2020. Massive ice control on permafrost coast erosion and sensitivity. Geophysical Research Letters, **47**: 9. doi:10.1029/2020GL087917.

Mackay, J.R., and Burn, C.R. 2005. A long-term field study (1951–2003) of ventifacts formed by katabatic winds at Paulatuk, western Arctic coast, Canada. Canadian Journal of Earth Sciences, **42**(9): 1615–1635. doi:10.1139/e05-061.

Malenfant, F. Whalen, D. Fraser, P. and van Proosdij, D 2022. Rapid coastal erosion of ice-bonded deposits on Pelly Island, southeastern Beaufort Sea, Inuvialuit Settlement Region, western Canadian Arctic. Canadian Journal of Earth Sciences **59**: (11)961–972. doi:10.1139/cjes-2021-0118.

Mann, P.J., Strauss, J., Palmtag, J., Dowdy, K., Ogneva, O., Fuchs, M., et al. 2022. Degrading permafrost river catchments and their impact on Arctic Ocean nearshore processes. Ambio, **51**: 439–455. doi:10.1007/s13280-021-01666-z.

Manson, G.K., Solomon, S.M., Forbes, D.L., Atkinson, D.E., and Craymer, M. 2005. Spatial variability of factors influencing coastal change in the Western Canadian Arctic. Geo-Marine Letters, 138–145. doi:10.1007/s00367-004-0195-9.

Nielsen, D., Pieper, P., Barkhordarian, A., Overduin, P., Ilyina, T., Brovkin, V., et al. 2022. Increase in Arctic coastal erosion and its sensitivity to warming in the twenty-first century. Nature Climate Change, **12**(3): 263–270. doi:10.1038/s41558-022-01281-0.

O'Rourke, M.J., 2017. Archaeological site vulnerability modelling: the influence of high impact storm events on models of shoreline erosion in the western Canadian Arctic. Open Archaeology, **3**(1): 1–16. doi:10.1515/opar-2017-0001.

Obu, J., Lantuit, H., Fritz, M., Pollard, W.H., Sachs, T., and Günther, F. 2016. Relation between planimetric and volumetric measurements of permafrost coast erosion: a case study from Herschel Island, western Canadian Arctic. Polar Research, **35**. doi:10.3402/polar.v35.30313.

Obu, J., Lantuit, H., Grosse, G., Günther, F., Sachs, T., Helm, V., and Fritz, M. 2017. Geomorphology coastal erosion and mass wasting along the Canadian Beaufort Sea based on annual airborne LiDAR elevation data. Geomorphology, **293**: 331–346. doi:10.1016/j.geomorph.2016.02.014.

Overduin, P.P., Strzelecki, M.C., Grigoriev, M.N., Couture, N., Lantuit, H., St-Hilaire-Gravel, D., et al. 2014. Coastal changes in the Arctic. Geological Society, **388**(1): 103–129. doi:10.1144/SP388.13.

O'Neill, H.B., Wolfe, S.A., and Duchesne, C. 2019. New ground ice maps for Canada using a paleogeographic modelling approach. The Cryosphere, **13**: 753–773. doi:10.5194/tc-13-753-2019.

Pardo-Pascual, J.E., Almonacid-Caballer, J., Ruiz, L.A., and Palomar-Vázquez, J. 2012. Automatic extraction of shorelines from Landsat TM and ETM+ multi-temporal images with subpixel precision. Remote Sensing of Environment, **123**: 1–11. doi:10.1016/j.rse.2012.02.024.

Paulic, J.E., Bartzen, B., Bennett, R., Conlan, K., Harwood, L., Howland, K., et al. 2011. Ecosystem overview report for the Darnley Bay Area of Interest (AOI). Canadian Science Advisory Secretariat research document 1919-50442011/062, Central and Arctic Region.

Pfalz, G. 2017. Lateral transport of sediment and organic matter, derived from coastal erosion, into the nearshore zone of the southern Beaufort Sea, Canada. Doctoral dissertation, Technische Universität Dresden.

Philipp, M., Dietz, A., Ullmann, T., and Kuenzer, C. 2022. Automated extraction of annual erosion rates for Arctic permafrost coasts using Sentinel-1, deep learning, and change vector analysis. Remote Sensing, **14**: 3656. doi:10.3390/rs14153656.

Ping, C.-L., Michaelson, G.J., Guo, M.T., Jorgenson, M.T., Kanevskiy, M., Shur, Y., et al. 2011. Soil carbon and material fluxes across the eroding Alaska Beaufort Sea coastline. Journal of Geophysical Research, **116**: G02004. doi:10.1029/2010JG001588.

Rachold, V., Eicken, H., Gordeev, V.V., Grigoriev, M.N., Hubberten, H.-W., Lisitzin, A.P., et al. 2004. Modern terrigenous organic carbon in-

put to the Arctic Ocean. *In* The organic carbon cycle in the Arctic Ocean. *Edited by* R. Stein and R.W Macdonald. pp. 33–55. doi:10.1007/978-3-642-18912-8_2.

Sankar, R.D., Murray, M.S., and Wells, P. 2019. Decadal scale patterns of shoreline variability in Paulatuk, N.W.T, Canada. Polar Geography, **42**: 196–213. doi:10.1080/1088937X.2019.1597395.

Schuster, P.F., Schaefer, K.M., Aiken, G.R., Antweiler, R.C., Dewild, J.F., Gryziec, J.D., et al. 2018. Permafrost stores a globally significant amount of mercury. Geophysical Research Letters, **45**(3): 1463–1471. doi:10.1002/2017GL075571.

Sergy, G. 2008. The coastline classification scheme for SCAT and oil spill response in Canada. *In* Proceedings of the 31st Arctic and Marine Oil Spill Program Technical Seminar. Environment Canada, Ottawa, ON. pp. 811–819.

Solomon, S.M. 2005. Spatial and temporal variability of coastline change in the Beaufort-Mackenzie region, Northwest Territories, Canada. Geo-Marine Letters, 127–137. doi:10.1007/s00367-004-0194-x.

St. Pierre, K.A., Zolkos, S., Shakil, S., Tank, S.E., St Louis, V.L., and Kokelj, S.V. 2018. Unprecedented increases in total and methyl mercury concentrations downstream of retrogressive thaw slumps in the Western Canadian Arctic. Environmental Science & Technology, **52**: 14099–14109.

Tanski, G., Wagner, D., Knoblauch, C., Fritz, M., Sachs, T., and Lantuit, H. 2019. Rapid CO_2 release from eroding permafrost in seawater. Geophysical Research Letters, **46**. doi:10.1029/2019GL084303.

Tarnocai, C., Kimble, J., and Broll, G. 2003. Determining carbon stocks in Cryosols using the Northern and Mid-Latitudes Soil Database. *Edited by* M. Philips, S. Springman and L. U. Arenson. A. A. Balkema, Lisse, Netherlands. pp. 1129–1134.

Vos, K., Splinter, K.D., Harley, M.D., Simmons, J.A., and Turner, I.L. 2019. CoastSat: a Google Earth engine-enabled Python toolkit to extract shorelines from publicly available satellite imagery. Environmental Modelling & Software, **122**: 104528.

Whalen, D., Forbes, D.L., Kostylev, V., Lim, M., Fraser, P., Nedimovic, M.R., and Stuckey, S. 2022. Mechanisms, volumetric assessment, and prognosis for rapid coastal erosion of Tuktoyaktuk Island, an important natural barrier for the harbour and community. Canadian Journal of Earth Sciences, **59**. doi:10.1139/cjes-2021-0101.

Yorath, C.J., Balkwill, H.R., and Klassen, R.W. 1975. Franklin Bay and Malloch Hill map-areas. District of Mackenzie. Geological Survey of Canada, Paper 74-36. doi:10.4095/102527.